Magnetic Resonance Imaging 58 (2019) 108–115

Contents lists available at ScienceDirect

Magnetic Resonance Imaging

journal homepage: www.elsevier.com/locate/mri

Original contribution

Eigenvector-based SPIRiT Parallel MR Imaging Reconstruction based on ℓ_p pseudo-norm Joint Total Variation

Jizhong Duan[a], Zhongwen Bao[a], Yu Liu[b,*]

[a] Faculty of Information Engineering and Automation, Kunming University of Science and Technology, Kunming 650500, China
[b] School of Microelectronics, Tianjin University, Tianjin 300072, China

ARTICLE INFO

Keywords:
Parallel Magnetic Resonance imaging
ESPIRiT
Joint Total Variation
ℓ_p pseudo-norm
Majorization Minimization method
Operator Splitting technique

MSC:
00-01
99-00

ABSTRACT

Parallel Magnetic Resonance (MR) imaging is a well-established acceleration technique based on the spatial sensitivities of array receivers. Eigenvector-based SPIRiT (ESPIRiT) is a new parallel MR imaging reconstruction method that combines the advantages of the SENSE and GRAPPA methods. It estimates multiple sets of the sensitivity maps from the calibration matrix that is constructed from the auto-calibration data. To improve the quality of the reconstructed image, we introduced the Total Variation (TV) and ℓ_p pseudo-norm Joint TV (ℓ_pJTV) regularization terms to the ESPIRiT model for parallel MR imaging reconstruction, which were solved by using the Operator Splitting (OS) method. The resulting denoising problems with the TV and ℓ_pJTV regularization terms were solved by exploiting the Majorization Minimization method. Simulation experiments on two in vivo data sets demonstrated that the proposed OS algorithm with the TV regularization term (OSTV) and OS algorithm with the ℓ_pJTV regularization term (OSℓ_pJTV) outperformed the conventional method with the ℓ_1 regularization term in terms of SNR and NRMSE. And the OSℓ_pJTV algorithm was slightly superior to the OSTV algorithm with the TV regularization term.

1. Introduction

Magnetic Resonance (MR) imaging is a non-invasive and non-ionizing imaging tool that provides good contrast between different soft tissues of the body compared to most other imaging methods. However, the speed of collecting the k-space data in MR imaging is fundamentally limited due to physical and physiological constraints [1]. Parallel MR imaging is a well-known acceleration technique that takes advantage of the spatial sensitivity of multiple array receivers to reduce the acquisition times of MR imaging. Over the past twenty years, many reconstruction algorithms for parallel MR imaging have been proposed. These reconstruction algorithms are divided into two major categories: algorithms using the coil sensitivity information explicitly such as SENSE [2,3], and algorithms utilizing the sensitivity information implicitly, which exploit the learned correlation between multiple channels in neighboring points in k-space, such as GRAPPA [4] and SPIRIT [5-7].

When the sensitivities are exact, SENSE allows optimal reconstruction. However, the sensitivities information with high accuracy is often very difficult to measure in practical applications [6]. On the other hand, algorithms based on learned correlations is ineffective for high acceleration factors, but are much more robust to errors [8]. To combine the advantages of the SENSE and GRAPPA approaches, the ESPIRiT model is proposed in Refs. [8-10] for parallel imaging reconstruction. In the ESPIRiT model, the sensitivity maps of the receive coils are estimated in the image domain as the main eigenvector of a related reconstruction operator, which is computed from the null space of a calibration matrix constructed from the auto-calibration data, whose null space encodes correlations between channels and neighboring points in k-space. In case of aliasing due to motion corruption, chemical shift, ghosting or a small Field of View (FOV), multiple sets of the sensitivity maps are necessary in reconstruction [10]. The ESPIRiT model is used to achieve high acceleration needed for 3D volumetric MR imaging [11,12]. In Ref. [13], the ESPIRiT model and virtual conjugate coils are used to estimating absolute-phase maps. In Refs. [10,8], the ℓ_1 regularization term based on the wavelet transform is used to promote the sparsity of the image components to be reconstructed. However, its reconstructed image exhibits slight artifacts.

To improve the quality of the image reconstructed by the ESPIRiT model, this paper proposes an Operator Splitting (OS) based method [14] for solving the ESPIRiT Parallel MR Imaging Reconstruction with the Total Variation (TV) regularization term [15,16]. The corresponding denoising problem with the TV regularization term can be solved efficiently by using the Alternating Direction Method of

* Corresponding author.
E-mail addresses: duanjz@kmust.edu.cn (J. Duan), baozhong.168@qq.com (Z. Bao), liuyu@tju.edu.cn (Y. Liu).

https://doi.org/10.1016/j.mri.2019.01.014
Received 7 November 2018; Received in revised form 23 December 2018; Accepted 14 January 2019

Multipliers (ADMM) [17] or split Bregman methods [18,16]. We also propose an OS based method for solving the ESPIRiT Parallel MR Imaging Reconstruction with the ℓ_p pseudo-norm Joint TV (ℓ_pJTV) regularization term [19,20]. The resulting denoising problem with the ℓ_pJTV regularization term can be solved by using the Majorization Minimization (MM) method [21-23].

The remainder of this paper is structured as follows. In Section 2, we briefly review the ESPIRiT model. Then, we present our proposed algorithm for solving the ESPIRiT Parallel MR Imaging Reconstruction problem with the ℓ_pJTV regularization term in Section 3. Simulated experimental results and analysis are provided in Section 4. Finally, Section 5 concludes this paper.

2. Overview of ESPIRiT

In the ESPIRiT model [8], the sensitivity information s_r at each spatial domain point r of the image can usually be obtained by solving the following problem:

$$\mathcal{G}_r s_r = s_r \tag{1}$$

where s_r is an eigenvector corresponding to $\mathcal{G}_r$'s eigenvalue "$=1$". The definition of $\mathcal{G}_r$ is:

$$\mathcal{G}_r = \mathcal{F}^{-1}\mathcal{W}\mathcal{F} \tag{2}$$

where $\mathcal{F} = I_C \otimes F_n \otimes F_m \in \mathbb{C}^{NC\times NC}$ is a matrix of 2D Fourier transforms for vectorized multi-coil images, F_m and F_n are Fourier transform matrices of m points and n points, respectively. The symbol "$\otimes$" represents the "Kronecker product". The I_C is the identity matrix of $C \times C$. $\mathcal{W}$ is a reconstruction operator, defined as follows:

$$\mathcal{W} = \left(\sum_r R_r^H R_r\right)^{-1} \sum_r R_r^H V_{\|} V_{\|}^H R_r \tag{3}$$

where R_r represents the operation of choosing a block of the k-space around the positions indexed by r. $V_{\|}$ is the row space spans of the calibration matrix A, which is constructed by sliding a window throughout the auto-calibration Signal (ACS) lines [8].

In the ESPIRiT model, the calibration matrix A has the null space vector, that is to say, k-space blocks are related, and the missing data can be reconstructed by the correlation between them [8]. The singular value decomposition (SVD) of the calibration matrix A is:

$$A = U\Sigma V^H \tag{4}$$

The columns of the V matrix in the SVD are a basis for the rows of A, and therefore basis for all the overlapping blocks in the calibration data. V can be separated into $V_{\perp}$ which spans the null space of A and $V_{\|}$ which spans its row space.

In some cases, errors in the acquisition lead to the appearance of multiple eigenvectors to eigenvalue "$=1$" or additional eigenvalues smaller than one, indicating signal components which cannot be explained in terms of the strict SENSE model. Therefore, the following model is proposed to obtain multiple sets of sensitivity information [8]:

$$\mathcal{G}_r = \sum_{j=1}^{J} \lambda_j(r) s_j(r) s_j^H(r) \tag{5}$$

where J denotes the number of sets of sensitivity information, and all $\lambda_j(r)$ are often close to one. $s_j(r)$ is the 'j'th set of sensitivity information with spatial position r. Rearranging all the positions' $s_j(r)$ to obtain a diagonal matrix $S_{cj} \in \mathbb{C}^{N\times N}$, a reconstruction model based on ESPIRiT is available:

$$y_c = PF\sum_{j=1}^{J} S_{cj} x_j \tag{6}$$

where $F = F_n \otimes F_m \in \mathbb{C}^{N\times N}$. $P \in \mathbb{R}^{M\times N}$ is the undersampling matrix ($M < N$, $N = m \times n$), whose rows are composed of the rows of the $N \times N$ identity matrix, which is equivalent to selecting the data of the corresponding position on the k-space. $y_c \in \mathbb{C}^M$ is the subsampled data of the 'c'th coil. $x_j \in \mathbb{C}^N$ is the 'j'th component of the image to be reconstructed. Eq. (6) can be solved by the least squares method.

Uecker et al. used the regularization technique to transform Eq. (6) into the following optimization problem [10,8]:

$$x = \arg\min_x \frac{1}{2}\sum_{c=1}^{C}\left\| y_c - PF\sum_{j=1}^{J} S_{cj}x_j \right\|_2^2 + \alpha\sum_{j=1}^{J}\|\Psi x_j\|_1 \tag{7}$$

where Ψ is the wavelet transform.

3. The proposed algorithm

3.1. Problem formulation

For convenience of expression, we represent the ESPIRiT reconstruction model in a more compact form:

$$y = \mathcal{P}\mathcal{F}\mathcal{S}x \tag{8}$$

where $\mathcal{P} = I_C \otimes P \in \mathbb{R}^{MC\times NC}$, $y = (y_1^T,\ldots,y_C^T)^T \in \mathbb{C}^{MC}$, $x = (x_1^T,\ldots,x_J^T)^T \in \mathbb{C}^{NJ}$. The matrix $\mathcal{S}$ consists of all S_{cj}:

$$\mathcal{S} = \begin{pmatrix} S_{11} & \cdots & S_{1J} \\ \vdots & \ddots & \vdots \\ S_{C1} & \cdots & S_{CJ} \end{pmatrix} \in \mathbb{C}^{NC\times NJ} \tag{9}$$

In order to improve the quality of reconstruction, the TV regularization term [15,16] is introduced, and the optimization problem is expressed as:

$$x = \arg\min_x \frac{1}{2}\|y - \mathcal{P}\mathcal{F}\mathcal{S}x\|_2^2 + \alpha\sum_{j=1}^{J}\|x_j\|_{\mathrm{TV}} \tag{10}$$

where $\|x_j\|_{\mathrm{TV}} = \|Dx_j\|_1 = \sum_{r=1}^{N}\|(Dx_j)_r\|$, $D = (D_h;D_v) \in \mathbb{R}^{2N\times N}$, D_h and D_v are first-order finite difference transforms in row and column directions, respectively. $D_h = D_n \otimes I_m \in \mathbb{R}^{N\times N}$, $D_v = I_n \otimes D_m \in \mathbb{R}^{N\times N}$. D_m is a circulant matrix of $m \times m$ and has the following structure:

$$D_m = \begin{pmatrix} -1 & 1 & & & 0 \\ 0 & -1 & 1 & & \\ & \ddots & \ddots & \ddots & \\ & & 0 & -1 & 1 \\ 1 & & & 0 & -1 \end{pmatrix} \tag{11}$$

Considering the Joint TV (JTV) regularization term [19,20] of the J image components, and using the ℓ_p pseudo-norm ($0 < p < 1$) [21-23] instead of the ℓ_1 norm, we can get the following optimization problem:

$$x = \arg\min_x \frac{1}{2}\|y - \mathcal{P}\mathcal{F}\mathcal{S}x\|_2^2 + \alpha\|\mathcal{D}x\|_p^p \tag{12}$$

where $\|\mathcal{D}x\|_p^p = \sum_r(\|(\mathcal{D}x)_r\|)^p$, $\mathcal{D} = I_J \otimes D \in \mathbb{R}^{2NJ\times NJ}$, I_J is the identity matrix of $J \times J$. $(\mathcal{D}x)_r \in \mathbb{C}^{2J\times 1}$ denotes a column vector composed of all points in which the spatial position r of $\mathcal{D}x$ is extracted, *i.e.*, $(\mathcal{D}x)_r = ((D_v x_1)_r,\ldots,(D_v x_J)_r, (D_h x_1)_r,\ldots,(D_h x_J)_r)^T$.

We specify the sparsity penalty as $\|\mathcal{D}x\|_p^p = \sum_r \varphi((\mathcal{D}x)_r) = \sum_r(\|(\mathcal{D}x)_r\|)^p$, and $\varphi(g) = \phi(\|g\|) = (\|g\|)^p$. And then, the problem (12) can be rewritten as:

$$x = \arg\min_x \frac{1}{2}\|y - \mathcal{P}\mathcal{F}\mathcal{S}x\|_2^2 + \alpha\sum_r \varphi((\mathcal{D}x)_r) \tag{13}$$

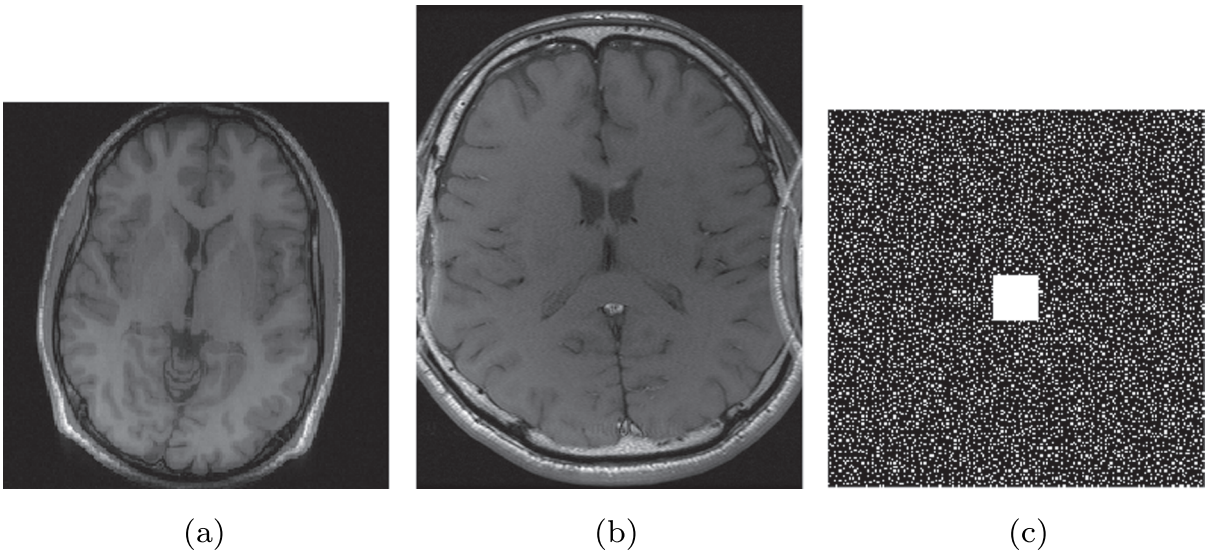

Fig. 1. The reference images from fully sampled data sets, (a) data1, (b) data2, and (c) Poisson-disc undersampling mask with 6× acceleration and 24 × 24 ACS lines.

3.2. The Operator Splitting method

Introducing the Operator Splitting (OS) technique [14], the problem (13) can be converted to:

$$z = x - \frac{1}{L}(\mathcal{P}\mathcal{F}\mathcal{S})^T(\mathcal{P}\mathcal{F}\mathcal{S}x - y) \tag{14}$$

$$x = \arg\min_x \frac{1}{2}\|x - z\|_2^2 + \lambda \sum_r \varphi((\mathcal{D}x)_r) \tag{15}$$

where L is a Lipschitz constant of the gradient of $\frac{1}{2}\|y - \mathcal{P}\mathcal{F}\mathcal{S}x\|_2^2$, and $\lambda = \alpha/L$.

The subproblem (15) is a denoising problem with the ℓ_pJTV regularization term, which can be solved by using the Majorization Minimization method (MMℓ_pJTV, detailed in the following section). When $p = 1$ and $J = 1$, the denoising problem (15) can be reduced to a denoising problem with the TV regularization term.

And then, we get an algorithm for solving the ESPIRiT parallel MR imaging reconstruction problem with the ℓ_pJTV regularization term. The whole process is presented in Algorithm 1, which is named as OSℓ_pJTV. In Algorithm 1, Steps 7 and 8 are the acceleration steps borrowed from the FISTA [24,25].

By using the OS technique, the problem (10) can be converted to:

$$z = x - \frac{1}{L}(\mathcal{P}\mathcal{F}\mathcal{S})^T(\mathcal{P}\mathcal{F}\mathcal{S}x - y) \tag{16}$$

$$x = \arg\min_x \frac{1}{2}\|x - z\|_2^2 + \lambda \sum_{j=1}^{J} \|x_j\|_{\mathrm{TV}} \tag{17}$$

The subproblem (17) can be converted to:

$$x_j = \arg\min_{x_j} \frac{1}{2}\|x_j - z_j\|_2^2 + \lambda \|x_j\|_{\mathrm{TV}}, \quad j = 1, \ldots, J \tag{18}$$

The denoising subproblem (18) can also be solved by using the MMℓ_pJTV ($p = 1$ and $J = 1$), then we get an OS based algorithm with the TV regularization term (OSTV) for the problem (10).

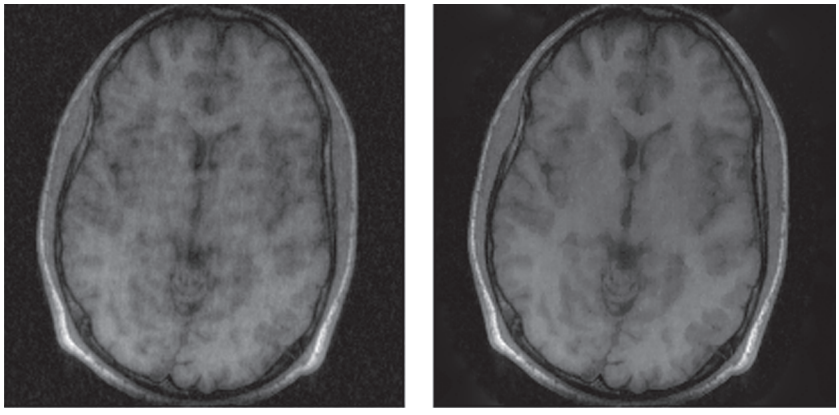

Fig. 2. For data1, (a) reconstructed images using a single set of sensitivity maps, (b) reconstructed images using two sets of sensitivity maps ($R = 6$, both using the TV regularization term, and all solved by using the OS method)

Algorithm 1. Operator Splitting method for solving the ESPIRiT parallel MR imaging Reconstruction problem with the ℓ_pJTV regularization term (OSℓ_pJTV).

Set $w^1 = 0, x^1 = 0, t^1 = 0, i = 0$

Input $y, \mathscr{P}, \mathscr{F}, \mathscr{S}$

repeat

  $i = i + 1$

  $z^{i+1} = w^i - \frac{1}{L}(\mathscr{P}\mathscr{F}\mathscr{S})^T(\mathscr{P}\mathscr{F}\mathscr{S}w^i - y)$

  Compute x^{i+1} in (15) using the MMℓ_pJTV algorithm

  $t^{i+1} = \frac{1+\sqrt{1+4(t^i)^2}}{2}$

  $w^{i+1} = x^{i+1} + \left(\frac{t^i - 1}{t^{i+1}}\right)(x^{i+1} - x^i)$

until some stopping criteria met

Output $x = x^{i+1}$

Algorithm 2. Majorization Minimization method for the denoising problem with the ℓ_pJTV regularization term (MMℓ_pJTV).

Set $x^1 = 0$

Input z^{i+1}

for $k = 1$ to K **do**

  for $r = 1$ to N **do**

    $u_r^{k+1} = (\mathscr{D}x^k)_r \cdot \max\left(1 - \frac{(\left\|(\mathscr{D}x^k)_r\right\|)^{p-2}}{\beta}, 0\right)$

  end for

  for $j = 1$ to J **do**

    $x_j^{k+1} = F^{-1}\left(\frac{F(z_j^{i+1} + \lambda\beta D^T u_j^{k+1})}{\lambda\beta F D^T D F^{-1} + I}\right)$

  end for

end for

Output $x^{i+1} = x^{K+1}$

3.3. Majorization Minimization method for the denoising problem with the ℓ_pJTV regularization term

We now derive an MM algorithm to solve the subproblem (15). We will consider the additive half-quadratic majorization [21-23] of the potential function φ, specified by:

$$\varphi(t) = \arg\min_x \frac{\beta}{2}\|s - t\|_2^2 + \psi(s) \tag{19}$$

where $s \in \mathbb{C}^{2J\times 1}$ and $t \in \mathbb{C}^{2J\times 1}$ are auxiliary vector variables. By definition, $\psi(s)$ is a matrix function that is dependent on $\varphi(t)$. Ref. [23] deduces the solution of Eq. (19) as:

$$s = t \cdot \max\left(1 - \frac{(\|t\|)^{p-2}}{\beta}, 0\right) \tag{20}$$

Then, the subproblem (15) can be rewritten as:

$$(x, u) = \arg\min_{x,u} \frac{1}{2}\|x - z\|_2^2 + \frac{\lambda\beta}{2}\|u - \mathcal{D}x\|_2^2 + \lambda\sum_r \psi(u_r) \tag{21}$$

where $u \in \mathbb{C}^{2NJ\times 1}$ is an auxiliary vector variable. The solution of the problem (21) involves the minimization with respect to both x and u. By using an alternating minimization algorithm, we alternatively minimize Eq. (21) with respect to each of the variables, assuming the other to be fixed, *i.e.*,

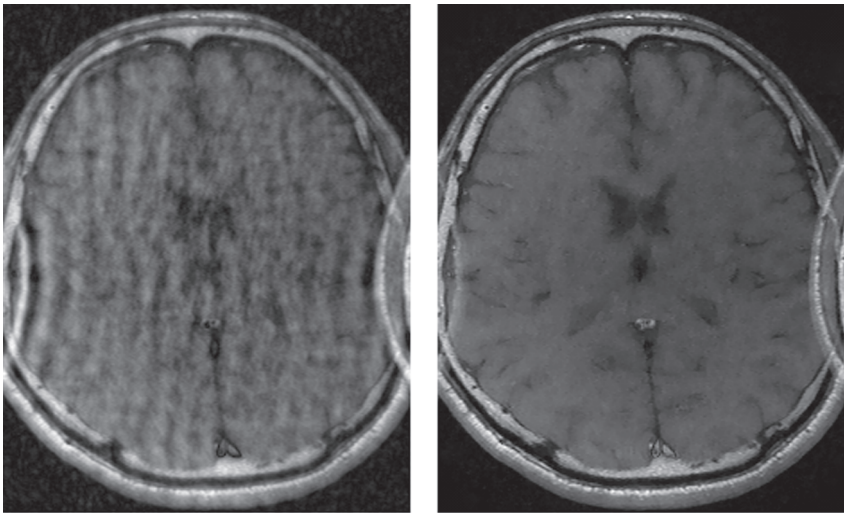

Fig. 3. For data2, (a) reconstructed images using a single set of sensitivity maps, (b) reconstructed images using two sets of sensitivity maps ($R = 6$, both using the TV regularization term, and all solved by using the OS method)

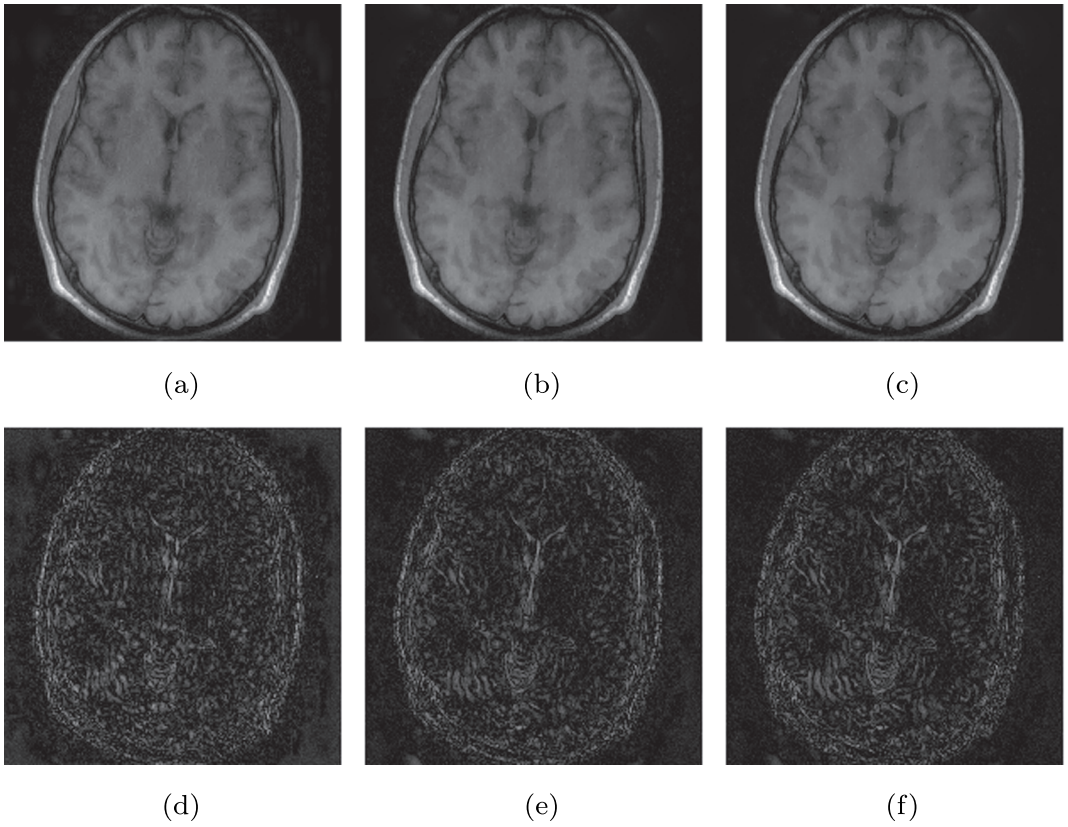

Fig. 4. Reconstructed parallel MR images for the data1 from the Poisson-disc undersampling with 6× acceleration and 24 × 24 ACS lines. (a), (b), and (c) are the reconstructed images by the OSL1, OSTV, and OSℓ_pJTV, respectively. (d), (e), and (f) are their corresponding error maps, respectively.

$$x = \arg\min_x \frac{1}{2}\|x - z\|_2^2 + \frac{\lambda\beta}{2}\|\mathcal{D}x - u\|_2^2 \tag{22}$$

$$u = \arg\min_u \frac{\lambda\beta}{2}\|u - \mathcal{D}x\|_2^2 + \lambda\sum_r \psi(u_r) \tag{23}$$

Because the variables in the subproblem (22) are independent for different components of x, each component variable can be solved separately:

$$x_j = \arg\min_{x_j} \frac{1}{2}\|x_j - z_j\|_2^2 + \frac{\lambda\beta}{2}\|\mathcal{D}x_j - u_j\|_2^2 \tag{24}$$

$D^TD = D_v^TD_v + D_h^TD_h$ is a block circulant matrix under periodic boundary condition and can be diagonalized by the two-dimensional discrete Fourier transform F. Therefore, the subproblem (24) can be easily computed by:

$$x_j = F^{-1}\left(\frac{F(z_j + \lambda\beta D^T u_j)}{\lambda\beta FD^T DF^{-1} + I}\right) \tag{25}$$

The subproblem (23) can be rewritten as:

$$u_r = \arg\min_{u_r} \frac{\beta}{2} \|u_r - (\mathcal{D}x)_r\|_2^2 + \psi(u_r) \tag{26}$$

According to Eq. (20), we can obtain the solution of the subproblem (26):

$$u_r = (\mathcal{D}x)_r \cdot \max\left(1 - \frac{(\|(\mathcal{D}x)_r\|)^{p-2}}{\beta}, 0\right) \tag{27}$$

Since the subproblems (22) and (23) can be efficiently solved, we get a new algorithm for solving the denoising problem (15). The whole process is presented in Algorithm 2, which is named as the Majorization Minimization method for solving the denoising problem with the ℓ_pJTV regularization term (MMℓ_pJTV). As analyzed above, the proposed MMℓ_pJTV exploits the fast Fourier transformation and componentwise operations to improve the efficiency.

4. Experimental results

4.1. Experimental setup

In the following experiments, we mainly compared the following three algorithms for solving the ESPIRiT model with two set of sensitivity maps, such as: the OS algorithm with the L1 regularization term (OSL1) for the problem (7) [8], the OS algorithm with the TV regularization term (OSTV) for the problem (10), and the OS algorithm with the ℓ_pJTV regularization term (OSℓ_pJTV) for the problem (12). We implemented all the compared algorithms in Matlab (MathWorks, Natick, MA).

To test the performance of all the compared the algorithms, we used two sets of fully sampled in vivo human brain data acquired by using an eight-channel head coil for multiple subjects, namely the data1 [6], and the data2 using a reduced Field of View (FOV) [8], which was smaller than the head of the subject, as shown in Fig. 1 (a), and (b). In order to generate testing data set, the fully sampled data sets are artificially down-sampled using the Cartesian Poisson-disc undersampling mask with R × acceleration (excluding ACS lines) such as in Fig. 1 (c) for reconstruction. In the following experiments, a calibration region of size 24 × 24 and an ESPIRiT kernel size of 6 × 6 were used for all the compared algorithms.

All of our experiments were carried out on a laptop with an Intel Core i5-3230M @ 2.6 GHz processor, 8 GB memory and Windows 10 operating system (64 bit). The regularization parameters of the compared algorithms were hand-tuned for SNR-optimal. In the following experiments, the Signal Noise Ratio (SNR) and Normalized Root Mean Squared Error (NRMSE) [6] were used to quantitatively evaluate the quality of reconstructed images, which are respectively defined as:

$$SNR = 10\log_{10}\left(\frac{Var}{MSE}\right) \tag{28}$$

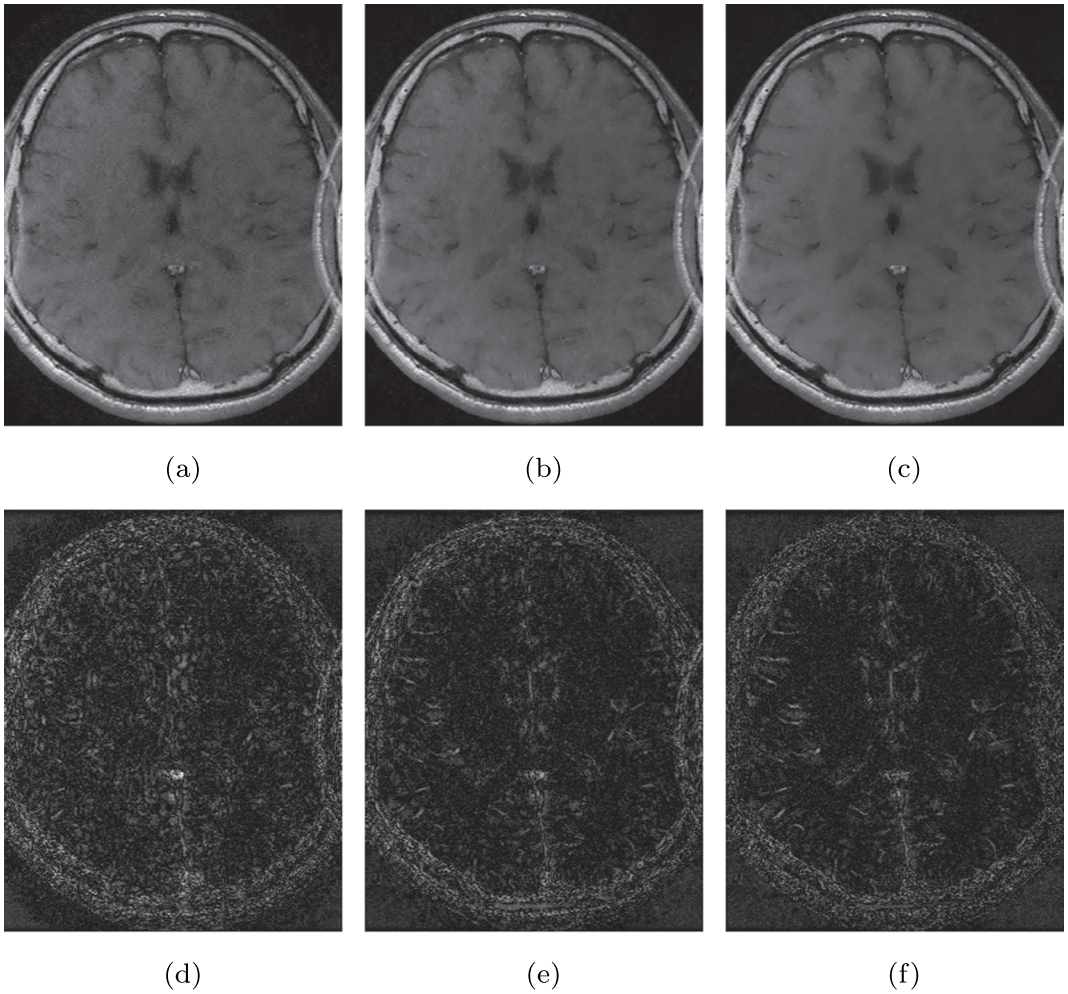

Fig. 5. Reconstructed parallel MR images for the data2 from the Poisson-disc undersampling with 6× acceleration and 24 × 24 ACS lines. (a), (b), and (c) are the reconstructed images by the OSL1, OSTV, and OSℓ_pJTV, respectively. (d), (e), and (f) are their corresponding error maps, respectively.

$$NRMSE = \frac{||\hat{x} - x||_2}{\max(x) - \min(x)} \quad (29)$$

where *MSE* represents the mean square error between the reconstructed image $\hat{x}$ and the reference image x calculated by using square root of sum of squares method from the fully sampled data set, and *Var* represents the variance of the reference image.

4.2. Comparison of algorithm performances of different sensitivity maps

First, we compare the algorithms using different sets of sensitivity maps. As shown in Fig. 2 (a), the image reconstructed by using only single set of maps exhibits very serious artifacts, so that the details of the image cannot be seen clearly. As shown in Fig. 2 (b), the quality of the image reconstructed by two sets of maps is greatly improved, and the image is relatively clear. This is because the single set of sensitivity map cannot correctly model the data, which leads to the loss of signal. while multiple sets of sensitivity maps can correctly model the data, so the reconstructed image's quality is relatively better. For the FOV smaller than the head of the subject, the advantage of using two sets of maps is more obvious, as shown in Fig. 3. Since the reconstruction quality using two sets of maps is better than using only one set of maps, we used two sets of maps for reconstruction in the following experiments.

4.3. Visual comparison

We visually compare the images reconstructed by the compared algorithms under the two data sets with an acceleration factor of 6, as shown in Figs. 4 and 5. Fig. 4 demonstrates the reconstructed images of the compared algorithms OSL1, OSTV, and OSℓ_pJTV for the data1, and their corresponding error maps. As shown in Fig. 4, the reconstructed image of the OSL1 has obvious blur artifacts. The quality of the image reconstructed by the OSTV is significantly better than that of the image reconstructed by the OSL1, and the OSℓ_pJTV further reduces the reconstruction error.

Fig. 5 demonstrates the reconstructed images of the compared algorithms OSL1, OSTV, and OSℓ_pJTV for the data2, and their corresponding error maps. As shown in Fig. 5, we can make a conclusion consistent with Fig. 4. In summary, the OSℓ_pJTV algorithm with the ℓ_pJTV regularization term always achieves best performance in terms of the reconstruction quality among the compared algorithms.

4.4. Performance comparison of compared algorithms with different acceleration factors

We also quantitatively evaluate the quality of the images reconstructed by the compared algorithms from the Cartesian undersampling at different acceleration factors of 3–12 for the data1, and the data2, respectively. Table 1 and Table 2 tabulate SNRs and NRMSEs of the reconstruction results with respect to the acceleration factors, and the SNR Improvements (ISNR) of the OSℓ_pJTV over the other competing algorithms. The higher the SNR value is, the better the reconstruction quality of the algorithm is. While the lower the NRMSE value is, the better the reconstruction quality of the algorithm is. As shown in Tables 1 and 2, we can see that the OSTV algorithm can achieve higher SNR than the OSL1 algorithm, and the OSℓ_pJTV algorithm outperforms the OSTV algorithm in terms of SNR and NRMSE. In detail, for the data1, the OSTV algorithm has average SNR improvements of 1.45 dB over the OSL1 algorithm, and the OSℓ_pJTV algorithm provides average SNR improvements of 2 dB and 0.55 dB over the OSL1 algorithm and the OSTV algorithm, respectively. For the data2, the OSTV algorithm has average SNR improvements of 1.14 dB over the OSL1 algorithm, and the OSℓ_pJTV algorithm provides average SNR improvements of 1.67 dB and 0.53 dB over the OSL1 algorithm and the OSTV algorithm, respectively. The observation about the performance of the compared algorithms is consistent with that in Section 4.3. Besides, we also can see that the reconstructed SNR by the OSℓ_pJTV at an acceleration factor of 6 is comparable to that by the conventional OSL1 algorithm at an acceleration factor of 4. That is to say, we can accelerate MR imaging by using the proposed algorithms.

Table 1
SNRs and NRMSEs of the compared algorithms for reconstructions from the Cartesian undersampling with 3–12× acceleration for the data1, and SNR Improvements (ISNR) of the OSℓ_pJTV over the other competing algorithms.

R	OSL1			OSTV			OSℓ_pJTV	
	SNR	ISNR	NRMSE	SNR	ISNR	NRMSE	SNR	NRMSE
3	20.24	2.63	0.0136	22.26	0.61	0.0110	22.87	0.0101
4	19.33	2.19	0.0151	20.75	0.77	0.0130	21.52	0.0118
5	18.57	2.03	0.0165	19.97	0.63	0.0142	20.60	0.0131
6	17.85	2.00	0.0179	19.30	0.55	0.0153	19.85	0.0143
7	17.09	1.79	0.0196	18.41	0.47	0.0169	18.88	0.0160
8	16.32	1.76	0.0214	17.62	0.46	0.0185	18.08	0.0175
10	15.35	1.82	0.0239	16.74	0.43	0.0205	17.17	0.0194
12	14.08	1.79	0.0277	15.40	0.47	0.0239	15.87	0.0226

Table 2
SNRs and NRMSEs of the compared algorithms for reconstructions from the Cartesian undersampling with 3–10× acceleration for the data2, and SNR Improvements (ISNR) of the OSℓ_pJTV over the other competing algorithms.

R	OSL1			OSTV			OSℓ_pJTV	
	SNR	ISNR	NRMSE	SNR	ISNR	NRMSE	SNR	NRMSE
3	18.97	0.86	0.0152	19.62	0.21	0.0142	19.83	0.0138
4	17.54	1.27	0.0180	18.44	0.37	0.0162	18.81	0.0155
5	16.64	1.41	0.0200	17.56	0.49	0.0180	18.05	0.0170
6	15.69	1.74	0.0223	16.87	0.56	0.0194	17.43	0.0182
7	14.86	1.78	0.0246	15.99	0.65	0.0215	16.64	0.0200
8	13.99	1.98	0.0273	15.34	0.63	0.0233	15.97	0.0216
9	13.17	2.14	0.0299	14.65	0.66	0.0254	15.31	0.0232
10	12.64	2.14	0.0318	14.12	0.66	0.0271	14.78	0.0247

5. Conclusion

To improve the quality of the reconstructed image, we introduced the TV and ℓ_pJTV regularization terms to the ESPIRiT model for Parallel MR Imaging Reconstruction, which was solved by using the OS method. The resulting denoising problem with the ℓ_pJTV regularization term can be solved by using the Majorization Minimization method. Simulation experiments on two in vivo data sets demonstrate that the proposed algorithms OSTV and OSℓ_pJTV outperform the conventional method with the ℓ_1 regularization term in terms of SNR and NRMSE. And the OSℓ_pJTV algorithm is slightly superior to the OSTV algorithm.

Acknowledgment

This work was supported by the National Natural Science Foundation of China under Grants 61861023, 61601385 and 61603319, Applied Basic Research Key Project of Yunnan (2018IB007), and the Scientific Research Foundation of Kunming University of Science and Technology (No. KKSY201703017). Thanks M. Lustig and M. Uecker for sharing their in vivo human brain data. The authors would like to thank the anonymous reviewers for their comments and suggestions.

References

[1] Lustig M, Donoho D, Pauly J M. Sparse MRI: the application of compressed sensing for rapid MR imaging. Magn Reson Med 2007;58(6):1182–95.
[2] Pruessmann K P, Weiger M, Bornert P, Boesiger P. Advances in sensitivity encoding with arbitrary k-space trajectories. Magn Reson Med 2001;46(4):638–51.
[3] Pruessmann K P, Weiger M, Scheidegger M B, Boesiger P. SENSE: sensitivity encoding for fast MRI. Magn Reson Med 1999;42(5):952–62.

[4] Griswold M A, Jakob P M, Heidemann R M, Nittka M, Jellus V, Wang J, et al. Generalized autocalibrating partially parallel acquisitions (GRAPPA). Magn Reson Med 2002;47(6):1202–10.
[5] Lustig M, Alley M, Vasanawala S, Donoho D, Pauly J. L1SPIR-It: autocalibrating parallel imaging compressed sensing. International Society for Magnetic Resonance in Medicine (ISMRM). 2009. p. 379.
[6] Lustig M, Pauly J M. SPIRIt: iterative self-consistent parallel imaging reconstruction from arbitrary k-space. Magn Reson Med 2010;64(2):457–71.
[7] Vasanawala S S, Alley M T, Hargreaves B A, Barth R A, Pauly J M, Lustig M. Improved pediatric MR imaging with compressed sensing. Radiology 2010;256(2):607–16.
[8] Uecker M, Lai P, Murphy M J, Virtue P, Elad M, Pauly J M, et al. ESPIRIt — an eigenvalue approach to autocalibrating parallel MRI: where SENSE, meets GRAPPA. Magn Reson Med 2014;71(3):990–1001.
[9] Lustig M, Lai P, Murphy M, Vasanawala S M, Elad M, Zhang J, et al. An eigen-vector approach to autocalibrating parallel MRI, where SENSE meets GRAPPA. International Society for Magnetic Resonance in Medicine (ISMRM). Canada: Montreal; 2011. p. 479.
[10] Uecker M, Virtue P, Vasanawala S S, Lustig M. ESPIRit reconstruction using soft SENSE. International Society for Magnetic Resonance in Medicine, Salt Lake City. 2013. p. 127.
[11] Lai P, Lustig M, Brau ACS, Vasanawala S S, Beatty P J, Alley M T. Efficient L1SPIRit reconstruction (ESPIRit) for highly accelerated 3D volumetric MRI with parallel imaging and compressed sensing. International Society for Magnetic Resonance in Medicine (ISMRM). 2010. 3154–3154.
[12] Lai P, Lustig M, Vasanawala S S, Brau A C. ESPIRit (efficient eigenvector-based L1SPIRit) for compressed sensing parallel imaging — theoretical interpretation and improved robustness for overlap. d FOV prescription. International Society for Magnetic Resonance in Medicine. 2011. p. 65.
[13] Uecker M, Lustig M. Estimating absolute-phase maps using ESPIRit and virtual conjugate coils. Magn Reson Med 2016;77(3):1201–7.
[14] Combettes P L, Wajs V R. Signal recovery by proximal forward-backward splitting. Multiscale Model. Sim 2005;4(4):1168–200.
[15] Rudin L I, Osher S, Fatemi E. Nonlinear total variation based noise removal algorithms. Physica D 1992;60(1-4):259–68.
[16] Duan J, Liu Y, Zhang L. Bregman iteration based efficient algorithm for mr image reconstruction from undersampled k-space data. IEEE Signal Proc Let 2013;20(8):831–4.
[17] Yang J, Zhang Y, Yin W. A fast alternating direction method for TVL1-l2 signal reconstruction from partial Fourier data. IEEE J Sel Topics Signal Process 2010;4(2):288–97.
[18] Goldstein T, Osher S. The split Bregman method for ℓ_1-regularized problems. SIAM J Imaging Sci 2009;2(2):323–43.
[19] Weller D, Ramani S, Fessler J A. Augmented Lagrangian with variable splitting for faster non-Cartesian l1-SPIRit MR image reconstruction. IEEE Trans Med Imag 2014;33(2):351–61.
[20] Duan J, Liu Y, Jing P. Efficient operator splitting algorithm for joint sparsity-regularized SPIRit-based parallel MR imaging reconstruction. Magn Reson Imaging 2018;46:81–9.
[21] Chartrand R. Fast algorithms for nonconvex compressive sensing: MRI reconstruction from very few data. IEEE International Symposium on Biomedical Imaging: From Nano to Macro (ISBI). 2009. p. 262–5.
[22] Hu Y, Lingala S G, Jacob M. A fast Majorize-Minimize algorithm for the recovery of sparse and low-rank matrices. IEEE Trans Image Process 2012;21(2):742–53.
[23] Mohsin Y Q, Ongie G, Jacob M. Iterative shrinkage algorithm for patch-smoothness regularized medical image recovery. IEEE Trans Med Imaging 2015;34(12):2417–28.
[24] Beck A, Teboulle M. Fast gradient-based algorithms for constrained total variation image denoising and deblurring problems. IEEE Trans Image Process 2009;18(11):2419–34.
[25] Beck A, Teboulle M. A fast iterative shrinkage-thresholding algorithm for linear inverse problems. SIAM J Imaging Sci 2009;2(1):183–202.